A 3D-printed sub-terahertz metallic surface-wave Luneburg lens multi-beam antenna

Nie, Boyu; Lu, Hongda; Skaik, Talal; Wang, Yi

DOI:
10.1109/TTHZ.2023.3242227

> T-TST-LET-12-2022-00198 <

A 3D-Printed Sub-terahertz Metallic Surface-wave Luneburg Lens Multi-beam Antenna

Boyu Nie, Hongda Lu, Talal Skaik, Yong Liu, and Yi Wang

[1]

***Abstract*—This letter presents an experimental realization of a sub-terahertz metallic gradient index (GRIN) lens multi-beam antenna operating at 355 GHz. The antenna is composed of a surface-wave Luneburg lens based on a bed of nails and a feeder array of nine WR-2.2 waveguides. The lens and the feeding structures are fabricated by the same high-precision 3D printing technique and are metalized using magnetron-sputtering gold coating. The antenna has been measured, showing good reflection coefficients below -12.5 dB at all ports and multiple independent beams covering a range of ±60°, which agree very well with the simulation. The measured gains are above 16 dBi and the scan loss is below 1.2 dB. This work demonstrates a novel manufacture and implementation approach for metallic multi-beam lens antennas at sub-terahertz frequencies.**

***Index Terms*— Sub-terahertz multi-beam antenna, metallic gradient index lens antenna, 3D printing, magnetron sputtering, surface-wave Luneburg lens.**

I. Introduction

PASSIVE multi-beam antennas have attracted much attention because of their low cost in the millimeter-wave (mmW) and sub-terahertz bands along with the application potential in the 5th-generation (5G) [1] and upcoming 6th-generation (6G) [2] wireless communication systems.

Multi-beam antennas in the mmW band based on the transmission line matrix networks [1] and quasi-optical networks [2] have been reported. The gradient index (GRIN) lenses are increasingly used as multi-beam networks owing to their compact structures and flexibility in generating directional beams. Metallic GRIN lenses have been reported in literatures at the mmW and higher frequency bands [3-13]. These antennas do not require dielectric materials often with associated dielectric losses at the high frequency. It should be noted that the high-resistivity silicon has been demonstrated to be an excellent low-loss material and used in all-dielectric terahertz lens [14]. However, its application scenarios may be limited because of the difficulty in the interconnecting with common waveguides and the stringent requirements for the micromachining process. The metallic GRIN lens, based on a different approach from the all-dielectric lens, allows secure and reliable interfaces with standard waveguides and still presents an attractive solution to multi-beam antenna at mmW and terahertz bands. However, it is difficult to realize the gradient refractive indices using traditional fully metallic structures. Design variations based on the artificial dielectric concept or metamaterial theory have been proposed. Examples include Luneburg lens realized by parallel plate waveguide (PPW) with gradual spacing [3-5], [11], GRIN lenses composed of the bed of nails or array of holes [6-11] and Luneburg lenses designed using the transformation-optics method [12], [13].

There have been a few excellent works on terahertz/sub-terahertz metallic E-plane-focused lenses realized by curved PPWs [4], [5]. However, there is no report on experimental realization of H-plane-focused multi-beam lens based on metallic periodic structures. Manufacture is a key challenge in meeting the tight tolerance requirement of few microns for the complex lens structure at terahertz/sub-terahertz. Silicon micromachining has been shown to be a viable technology in these frequencies for antenna elements [15-17] and arrays [18-22], but the etching process limits the possibility and flexibility of using structures of varying height. 3D printing affords more manufacture flexibility with its free-forming capability. Recently, high-precision 3D printing technology with 5 - 20 μm nominal dimensional tolerances has been demonstrated on sub-terahertz passive devices such as horn antenna [23] and filter [24]. However, the use of 3D printing on sub-terahertz multi-beam antenna has not been attempted before to the best of our knowledge.

In this letter, a metallic surface-wave Luneburg lens multi-beam antenna at 355 GHz based on non-uniform bed of nails is proposed, realized and experimentally verified for the first time using a high-precision 3D printing technique. Both the lens and the feeding waveguide array are printed and gold-coated. Its performance has been experimentally verified.

II. Design and Fabrication

A. Antenna structure and principle

The antenna is composed of a surface-wave Luneburg lens and an array of nine feeding waveguides. The feeding waveguide array is composed of two parts: waveguide grooves fabricated together with the lens by 3D printing, and a cover manufactured by CNC machining. The diagram of the antenna structure and the definitions of the dimensional parameters are given in Fig. 1(a) and (b). The lens consists of a bed of nails which support the transmission of the surface wave at 355 GHz. The Luneburg's law is used in the design and can be expressed as (1),

This work was supported by the National Natural Science Foundation of China under Grants 62271047, 61901040 and 12173006, and the U.K. Engineering and Physical Science Research Council under Grants EP/S013113/1 and EP/P020615/1. (Corresponding author: Hongda Lu).

Boyu Nie, Hongda Lu and Yong Liu are with the School of Integrated Circuits and Electronics, Beijing Institute of Technology, Beijing 100081, China. (e-mail: luhongda@bit.edu.cn).

Talal Skaik and Yi Wang are with the School of Electrical Electronic and Systems Engineering, University of Birmingham, Birmingham B15 2TT, U.K.

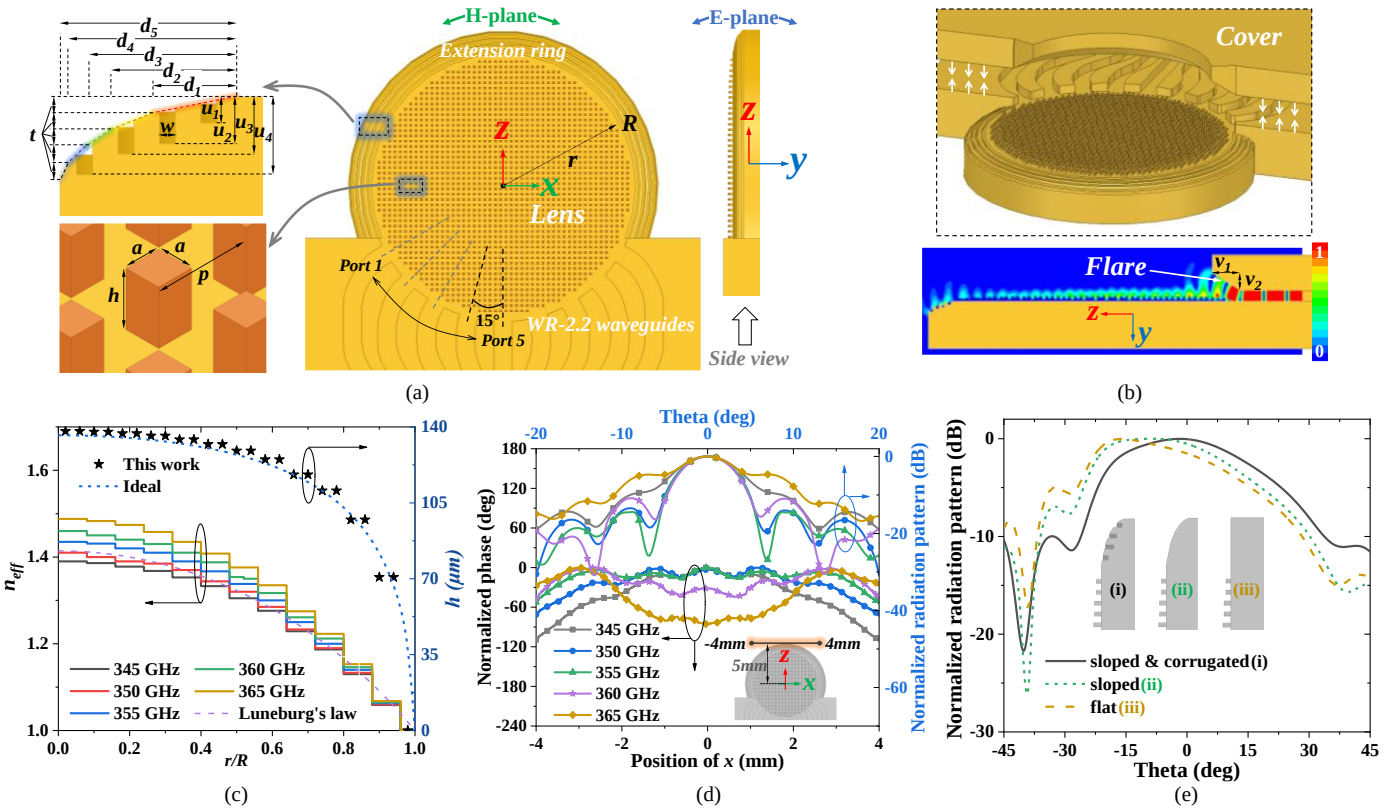

Fig. 1. (a) Diagram of the proposed lens multi-beam antenna. (b) Diagram of the waveguide cover and the E-field from waveguide to surface-wave lens. (c) Height profile of the bed of nails and refractive index profile of the surface-wave lens. (d) Phase distributions on lens antenna aperture and corresponding radiation patterns. (e) E-plane radiation patterns for different extension ring structures.

$$n = \sqrt{2 - \left(\frac{r}{R}\right)^2} \tag{1}$$

where n is the refractive index as a function of r and r/R is the normalized radius of the lens. The bed of nails acts as a slow wave structure. Its propagation constant increases with the pin height. The relationship between the effective refractive index n and the dimensions of the nails is given in (2) [6],

$$h = \frac{\arctan\left(\frac{p\sqrt{n^2-1}}{p-a}\right)}{k_0} \tag{2}$$

where k_0 is the wavenumber in free space.

Here, one major advantage of 3D printing is that the height of the nails can be varied without increasing the fabrication complexity. By taking advantage of this, the distribution of the heights of the nails is designed to be discrete as plotted in Fig. 1(c). As shown in Fig. 1(c), the realized refractive index profile of the lens agrees well with the Luneburg's law at 355 GHz and gradually varies with frequency because of the dispersion effect of the bed of nails. Fig. 1(d) shows the influence of dispersion on the aperture phase distribution and the radiation pattern of the lens antenna. As can be observed, the phase distributions at 350, 355 and 360 GHz are relatively uniform, which ensures the directional radiation requirement is met in the band from 350 to 360 GHz. In addition, as an attempt to point the E-plane radiation pattern close to 0°, a sloped corrugated extension ring is added around the lens, as shown in Fig. 1(a). To illustrate the effect of the extension ring, the E-plane radiation patterns for three different extension structures - flat, sloped and sloped corrugated - are compared in Fig. 1(e) in simulation. It is evident that the proposed extension ring re-point the E-plane beam. The lens antenna is fed by standard WR-2.2 waveguides connected with the test instruments. It should be noted that a flare structure is added at the interface between the rectangular waveguide and the bed of nails to realize an effective transition from the TE_{10} waveguide mode to TM surface-wave mode, as shown in Fig. 1(b). Nine waveguide sections are arranged with 15° angle increment to support a beam scanning range of ±60°. The dimensional parameters in Fig. 1(a) and (b) are optimized to be: R = 4000 μm, a = 60 μm, p = 160 μm, d_1 = 330 μm, d_2 = 490 μm, d_3 = 590 μm, d_4 = 655 μm, d_5 = 685 μm, u_1 = 100 μm, u_2 = 180 μm, u_3 = 220 μm, u_4 = 300 μm, t = 65 μm, w = 60 μm, v_1 = 800 μm, v_2 = 500 μm.

B. Fabrication

The prototype in Fig. 2 was fabricated by Stereolithography (SLA) 3D printing process. The lens and the feeding waveguides were co-printed with HTL resin by using a high-precision 3D printer (nanoArch S140, BMF), as shown in Fig. 2(a). The total size of the printed antenna device is 14 mm × 14 mm ×1.6 mm. The dimensions of the printed device show a high accuracy with an error between -/+ 5 μm. The printed

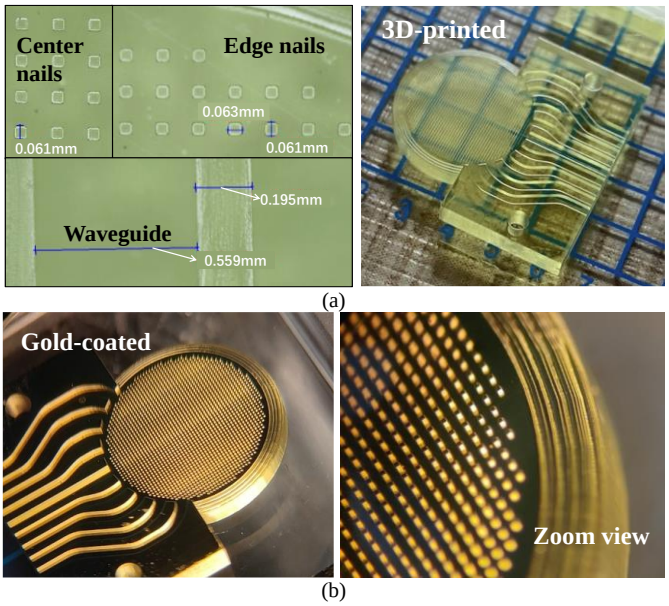

Fig. 2. Photographs of the antenna: (a) As printed and (b) after gold-coating.

device was then coated with 500 nm-thickness gold by magnetron sputtering to achieve the metal boundary of the multi-beam antenna as shown in Fig. 2(b).

III. Results and Discussion

To experimentally verify the multi-beam radiation characteristics of the proposed lens antenna, the radiation patterns excited from different ports and the reflection coefficients are measured. As shown in Fig. 3 (a), the test fixture and a connector containing a 90° waveguide bend between the antenna under test (AUT) and the UG-387 test flange are designed and CNC machined to support the measurements. At the interface between the fixture and connector, there are two pins on the fixture side and a row of pin holes on the connector side for the precise alignments during the port switching. Because of the space constraint, matched loads were not used on the unconnected ports. Due to the shieling effect of the waveguides, the interaction between the ports should not have any major impact on the impedance matching and radiation performance of each channel. As shown in Fig. 3(b), the simulated mutual couplings between ports are almost below -30 dB across the band from 350 to 360 GHz. It is noteworthy from Fig. 3(c) that although the impedance matching bandwidth can cover beyond 330 to 380 GHz, the gain drop outside the band from 350 to 360 GHz is significant. Therefore, the test of the radiation performances focuses on the band from 350 to 360 GHz.

The reflection coefficients are measured by a vector network analyzer (Keysight N5247B PNA-X) with sub-terahertz extenders (VDI WM570). Considering the symmetry of the antenna structure, only the reflection coefficients at port 1 to 5 are measured. The measured reflection coefficient for port 1 over the band from 330 to 380 GHz is given in Fig. 3(c) for the comparison with simulation. The results for the other ports in the band from 350 to 360 GHz are plotted in Fig. 3(d). The measured reflection coefficients are all below -12.5 dB,

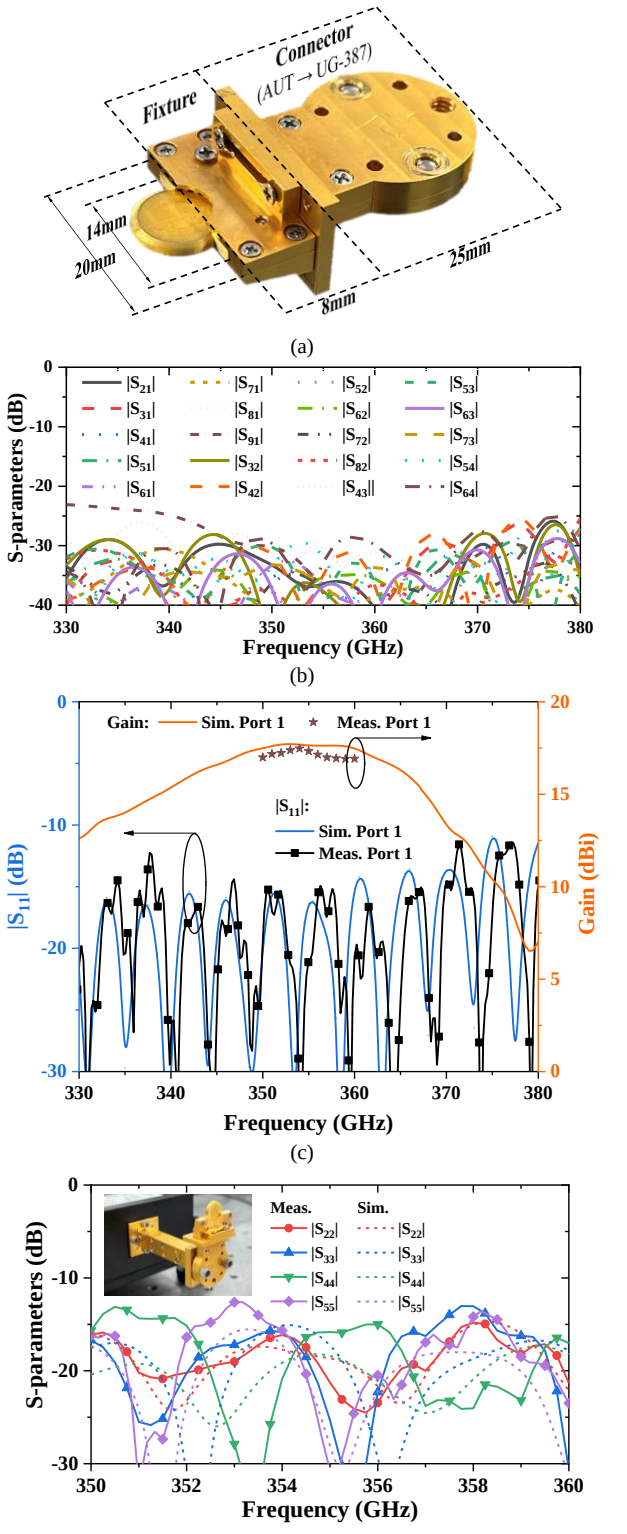

Fig. 3. (a) Photograph of antenna fixture and connector between AUT and UG-387 flange. (b) Simulated mutual couplings between ports. (c) Reflection coefficient and gain for port 1 from 330 to 380 GHz (d) Reflection coefficients for port 2, 3, 4 and 5 from 350 to 360 GHz.

agreeing well with the simulated results.

The radiation pattern test setup is composed of a rotator, a transmitting horn operating in the WR2.2 band and the antenna under test (AUT), as shown in Fig. 4(a). The H-plane multi-beam radiation patterns are plotted in Fig. 4(b) and (c).

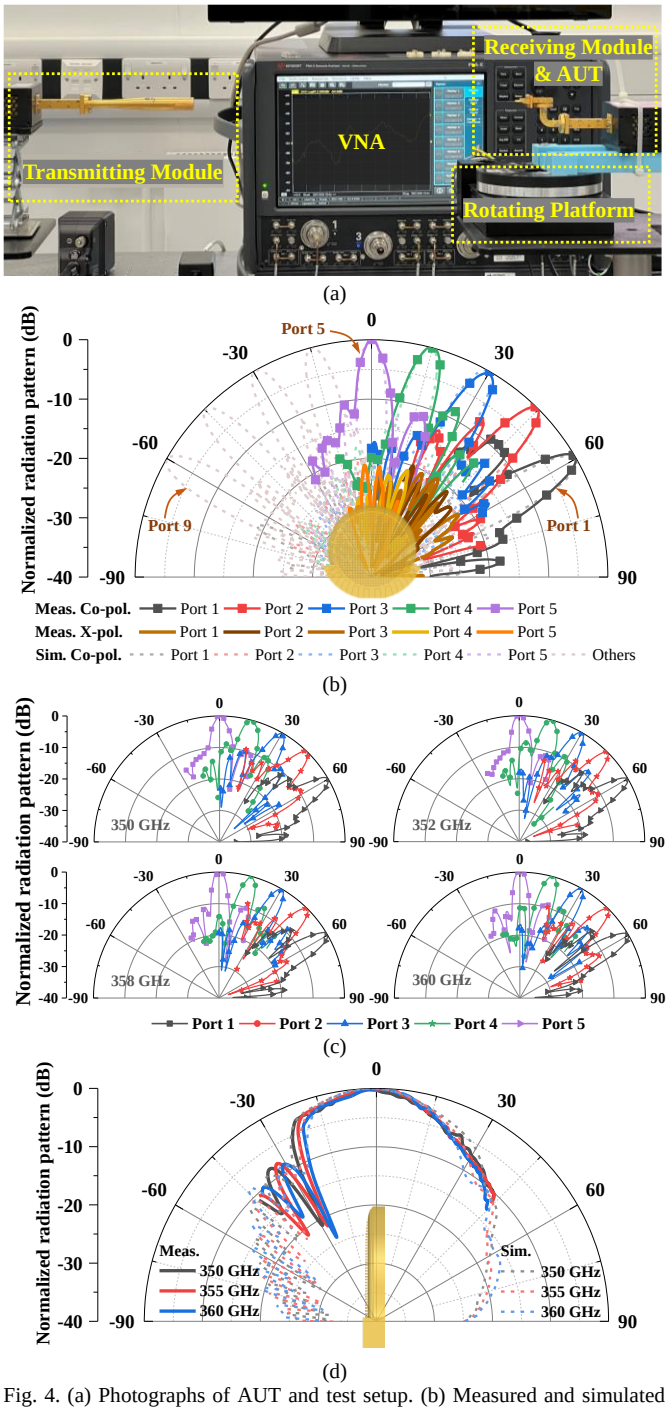

Fig. 4. (a) Photographs of AUT and test setup. (b) Measured and simulated H-plane radiation patterns at 355 GHz. (c) Measured H-plane radiation patterns at 350, 352, 358 and 360 GHz. (d) Measured and simulated E-plane radiation patterns.

The measured angular range of the beams are from -30° to +30°, enough to cover the main lobe and first sidelobe. Fig. 4(b) shows the measured co- and cross-polarization patterns at 355 GHz excited at port 1 to 5, respectively. The multi-beam patterns agree very well with the simulation especially for the main lobes. The sidelobe levels of the 15° and 60° beams are slightly higher than -10 dB. The H-plane half-power beamwidths for the tested ports are between 5.7° and 6.3°. The cross-polarization level for all the beams is below -20 dB, indicating a good linear polarization performance. The realized gain at 355 GHz is measured by the comparison method. The gains of the 0°, 15°, 30°, 45° and 60° beams are 17.3, 17.1, 16.7, 16.4 and 16.1 dBi, respectively. The multi-beam scan loss is lower than 1.2 dB. The gains for 0° beam at other frequencies in the band from 350 to 360 GHz are also measured and given in Fig. 3(c) as a comparison with the simulated results. The co-polarization radiation patterns at the lower and higher frequencies of 350, 352, 358 and 360 GHz are also measured and given in Fig. 4(c), which show similar multi-beam characteristics. The measured E-plane radiation patterns with beamwidths more than 32° in Fig. 4(d) indicate that the fan-beams are obtained and the maximum radiation directions in the E-plane are close to 0°, as expected. This is the first attempt on a H-plane-focused sub-terahertz fully metallic multi-beam lens antenna. Although its operating bandwidth is narrower than those metallic lens antennas based on PPW loaded with nails or holes [7-9], the surface-wave structure in this work, composed of bed of nails without cover, represents an easier solution to be realized at terahertz frequency.

IV. Conclusion

A 355 GHz surface-wave metallic Luneburg lens multi-beam antenna has been demonstrated. High-precision 3D printing has been used to manufacture the complex lens structure, with varying height of the periodic nails, together with its multi-port feeders for the first time. Good impedance matchings at all the feeding ports have been obtained with the measured reflection coefficients below -12.5 dB over the band from 350 GHz to 360 GHz. The multiple beams in the angle range of ±60° with their gains above 16 dBi and scan loss below 1.2 dB have been exhibited from the measured radiation patterns. With the modified edge ring structure, the E-plane radiation patterns with the maximum points close to 0° have been observed. The excellent agreement between the design and measured results demonstrates the feasibility of the proposed sub-terahertz metallic multi-beam antenna and the capability of the high-precision 3D printing technique.

References

[1] W. Hong, Z. H. Jiang, C. Yu, J. Zhou, P. Chen, Z. Yu, H. Zhang, B. Yang, X. Pang, M. Jiang, Y. Cheng, M. K. T. Al-Nuaimi, Y. Zhang, J. Chen, and S. He, "Multibeam Antenna Technologies for 5G Wireless Communications," IEEE Trans. Antennas Propag., vol. 65, no. 12, pp. 6231-6249, Dec, 2017.

[2] Y. J. Guo, M. Ansari, R. W. Ziolkowski, and N. J. G. Fonseca, "Quasi-Optical Multi-Beam Antenna Technologies for B5G and 6G mmWave and THz Networks: A Review," IEEE Open Journal of Antennas and Propagation, vol. 2, pp. 807-830, Jul, 2021.

[3] C. Hua, X. Wu, N. Yang, and W. Wu, "Air-Filled Parallel-Plate Cylindrical Modified Luneburg Lens Antenna for Multiple-Beam Scanning at Millimeter-Wave Frequencies," IEEE Trans. Microw. Theory Techn., vol. 61, no. 1, pp. 436-443, Jan, 2013.

[4] K. Sato, and Y. Monnai, "Terahertz Beam Steering Based on Trajectory Deflection in Dielectric-Free Luneburg Lens," IEEE Trans. THz Sci. Technol., vol. 10, no. 3, pp. 229-236, May, 2020.

[5] K. Sato, and Y. Monnai, "Two-Dimensional Terahertz Beam Steering Based on Trajectory Deflection of Leaky-Mode," IEEE Trans. THz Sci. Technol., vol. 11, no. 6, pp. 676-683, Nov, 2021.

[6] P. Young-Jin, A. Herschlein, and W. Wiesbeck, "A photonic bandgap (PBG) structure for guiding and suppressing surface waves in millimeter-

wave antennas," IEEE Trans. Microw. Theory Techn., vol. 49, no. 10, pp. 1854-1859, Oct, 2001.

[7] O. Quevedo-Teruel, J. Miao, M. Mattsson, A. Algaba-Brazalez, M. Johansson, and L. Manholm, "Glide-Symmetric Fully Metallic Luneburg Lens for 5G Communications at Ka-Band," IEEE Antennas Wireless Propag. Lett., vol. 17, no. 9, pp. 1588-1592, Sep, 2018.

[8] H. Lu, Z. Liu, Y. Liu, H. Ni, and X. Lv, "Compact Air-Filled Luneburg Lens Antennas Based on Almost-Parallel Plate Waveguide Loaded With Equal-Sized Metallic Posts," IEEE Trans. Antennas Propag., vol. 67, no. 11, pp. 6829-6838, Nov, 2019.

[9] H. Lu, Z. Liu, J. Liu, G. Wu, Y. Liu, and X. Lv, "Fully Metallic Anisotropic Lens Crossover-in-Antenna Based on Parallel Plate Waveguide Loaded With Uniform Posts," IEEE Trans. Antennas Propag., vol. 68, no. 7, pp. 5061-5070, Jul, 2020.

[10] J. Zhao, Y.-D. Wang, L.-Z. Yin, F.-Y. Han, T.-J. Huang, and P.-K. Liu, "Bifunctional Luneburg–fish-eye lens based on the manipulation of spoof surface plasmons," Opt. Lett., vol. 46, no. 6, pp. 1389-1392, March, 2021.

[11] J. Liu, H. Lu, Z. Dong, Z. Liu, Y. Liu, and X. Lv, "Fully Metallic Dual-Polarized Luneburg Lens Antenna Based on Gradient Parallel Plate Waveguide Loaded With Nonuniform Nail," IEEE Trans. Antennas Propag., vol. 70, no. 1, pp. 697-701, Jan, 2022.

[12] Q. Liao, N. J. G. Fonseca, and O. Quevedo-Teruel, "Compact Multibeam Fully Metallic Geodesic Luneburg Lens Antenna Based on Non-Euclidean Transformation Optics," IEEE Trans. Antennas Propag., vol. 66, no. 12, pp. 7383-7388, Dec, 2018.

[13] N. J. G. Fonseca, Q. Liao, and O. Quevedo-Teruel, "Equivalent Planar Lens Ray-Tracing Model to Design Modulated Geodesic Lenses Using Non-Euclidean Transformation Optics," IEEE Trans. Antennas Propag., vol. 68, no. 5, pp. 3410-3422, May, 2020.

[14] D. Headland, W. Withayachumnankul, R. Yamada, M. Fujita, and T. Nagatsuma, "Terahertz multi-beam antenna using photonic crystal waveguide and Luneburg lens," APL Photonics, vol. 3, no. 12, pp. 126105:1-126105:18, Dec, 2018.

[15] J. Hu, W. T. Lv, H. T. Zhu, Z. Lou, D. Liu, J. Q. Ding, and S. C. Shi, "Design, Uncertainty Analysis, and Measurement of a Silicon-Based Platelet THz Corrugated Horn," IEEE Trans. Antennas Propag., vol. 70, no. 7, pp. 5897-5901, Jul, 2022.

[16] Y. Liu, H. Lu, Y. Wu, M. Cui, B. Li, P. Zhao, and X. Lv, "Millimeterwave and Terahertz Waveguide-Fed Circularly Polarized Antipodal Curvedly Tapered Slot Antennas," IEEE Trans. Antennas Propag., vol. 64, no. 5, pp. 1607-1614, May, 2016.

[17] V. M. Lubecke, K. Mizuno, and G. M. Rebeiz, "Micromachining for terahertz applications," IEEE Trans. Microwave Theory Tech., vol. 46, no. 11, pp. 1821-1831, Nov, 1998.

[18] L. Chang, Y. Li, Z. Zhang, X. Li, S. Wang, and Z. Feng, "Low-Sidelobe Air-Filled Slot Array Fabricated Using Silicon Micromachining Technology for Millimeter-Wave Application," IEEE Trans. Antennas Propag., vol. 65, no. 8, pp. 4067-4074, Aug, 2017.

[19] L. Chang, Y. Li, Z. Zhang, S. Wang, and Z. Feng, "Planar Air-Filled Terahertz Antenna Array Based on Channelized Coplanar Waveguide Using Hierarchical Silicon Bulk Micromachining," IEEE Trans. Antennas Propag., vol. 66, no. 10, pp. 5318-5325, Oct, 2018.

[20] A. Gomez-Torrent, M. García-Vigueras, L. L. Coq, A. Mahmoud, M. Ettorre, R. Sauleau, and J. Oberhammer, "A Low-Profile and High-Gain Frequency Beam Steering Subterahertz Antenna Enabled by Silicon Micromachining," IEEE Trans. Antennas Propag., vol. 68, no. 2, pp. 672-682, Feb, 2020.

[21] A. Gomez-Torrent, T. Tomura, W. Kuramoto, J. Hirokawa, I. Watanabe, A. Kasamatsu, and J. Oberhammer, "A 38 dB Gain, Low-Loss, Flat Array Antenna for 320–400 GHz Enabled by Silicon-on-Insulator Micromachining," IEEE Trans. Antennas Propag., vol. 68, no. 6, pp. 4450-4458, Jun, 2020.

[22] S. S. Yao, Y. J. Cheng, M. M. Zhou, Y. F. Wu, and Y. Fan, "D-Band Wideband Air-Filled Plate Array Antenna With Multistage Impedance Matching Based on MEMS Micromachining Technology," IEEE Trans. Antennas Propag., vol. 68, no. 6, pp. 4502-4511, Jun, 2020.

[23] B. Zhang, Z. Zhan, Y. Cao, H. Gulan, P. Linnér, J. Sun, T. Zwick, and H. Zirath, "Metallic 3-D Printed Antennas for Millimeter- and Submillimeter Wave Applications," IEEE Trans. THz Sci. Technol., vol. 6, no. 4, pp. 592-600, Jul, 2016.

[24] T. Skaik, Y. Wang, M. Salek, P. Hunyor, H. Wang, P. G. Huggard, T. Starke, M. Attallah, and R. Martinez, "A 3-D Printed 300 GHz Waveguide Cavity Filter by Micro Laser Sintering," IEEE Trans. THz Sci. Technol., vol. 12, no. 3, pp. 274-281, May, 2022.